Design and Fabrication of Magnetorheological Elastomer Vibration Isolator

Ubaidillah, Syamsul Hadi[*]*, Harjana*
Universitas Sebelas Maret, Surakarta, Indonesia
National Center for Sustainable Transportation Technology, Bandung, Indonesia

Khairunnisa Hairuddin, Saiful Amri Mazlan
Vehicle System Engineering, Malaysia-Japan International Institute of Technology, Universiti Teknologi Malaysia

[*]*ubaidillah@uns.ac.id*

ABSTRACT

Universal vibration isolator uses thin layer magnetorheological elastomers (MREs). This article presents a development of cone-shaped MREs based vibration isolator featuring thick MREs. This work begins with a prototype design, magnetic circuit evaluation, prototype fabrication, and cyclic load preliminary tests. In this article, finite element magnetic method (FEMM) was used to design the electromagnetic circuit. An innovative magnetic circuit design is proposed for MREs isolator with cone shape MREs materials. MREs and shaft are adopted as magnetic core together with steel housing. MREs are placed at the end of each shaft and attached to the housing to form an enclosed magnetic path in the isolator. FEMM results showed that this novel design can provide sufficient magnetic field to all MREs region. Finally, the influence of input current to the MREs isolator on magnetic field strength is investigated. It is found that the magnetic field in MREs isolator increase with the increase of the input current.

Keywords: *Magnetorheological Elastomers Isolator, Electromagnetic Circuit, Mounting.*

ISSN 1823- 5514, eISSN 2550-164X

Received for review: 2017-05-09
Accepted for publication: 2017-06-01
Published: 2018-05-15

Introduction

Magnetorheological elastomers (MREs) are classified as a new comparable smart material whose mechanical property can be changed quickly and reversibly with the presentation of the magnetic field [1,2]. These materials are composed of magnetizable particle that embedded in a low-permeability matrix with additives [3,4,5]. The polymer matrix that commonly used for MREs is synthetic or natural rubber [5,6]. Meanwhile, the magnetization particle is widely carbonyl iron [6,7]. MREs are the solid-state analogs of MR fluids (MRFs) [1,4,7] because the matrix of MREs is solid form as compared to MRFs using a carrier oil. Therefore, MREs can avert shortcoming of MRFs in term of particle sedimentation and seal issues while providing stability for passive application [3,4,5].

The most important feature of MREs material is its controllable modulus. In general, the stiffness and damping properties of MREs will continuously vary under magnetic field. According to previous research conducted by Li et al. [10], the magnetic circuit enables MREs shear modulus change to 0.2 MPa about 100% under 0.7 T which compared to zero state 0.1 MPa. Once the magnetic field is removed, MREs will instantly change to its original properties [9,11,12]. Such controllable MREs offer great potential for various applications as vibration absorber, automotive bushing, propeller shaft absorber, variable spring rate, tire pressure control, impact element, medical rehabilitation and remotely controllable attachment [13].

MREs material offers a vast potential as vibration mitigation devices with field dependent modulus properties. Conventional rubber vibration isolators become the most choices to employ MREs material for adaptive performance [14,15,16,17,18,12]. Lerner and Cunefare [14] designed MREs-based vibration absorber with three different configurations that excited in shear, squeeze and compression modes. Behrooz et al. [15] prototyped a variable stiffness and damping isolator (VSDI) for structural vibration mitigation purpose. A comprehensive review of current MREs-based devices can be found in Li et al. [12]. Deng et al. [16] designed an adaptively tuned vibration absorber (ATVA) that capable to shift natural frequency from 27.5 Hz t0 40 Hz. Despite the innovative designs presented, MREs above isolators have a similar design concept with conventional isolator. Also, most of the devices only flexible in unidirectional action due to the layered design. This fact is mainly due to the difficulty to provide an ample magnetic field for MREs. To date, designing MREs devices with innovative shape remain challenging.

MREs material has been proposed to be used in isolation system to overcome the weaknesses of the conventional isolation system. Since the primary function of the isolator is its horizontal stiffness, isolator should sufficiently maintain the stiffness in low condition. Low lateral stiffness is

required to decouple seismic motion efficiently. This condition will enable the isolator to attenuate the fundamental period of structure beyond resonance states under typical vibration range [19]. Also, it is essential to maintain the necessary of isolator by having high vertical stiffness regardless the modification in horizontal stiffness. It is mainly based on the requirements for the isolator to be installed underneath the structure.

This article features a critical aspect in designing MREs vibration isolator, that is, magnetic circuit design. An innovative MREs vibration isolator structure is proposed to fulfill the intention of flexible isolator engagement in civil engineering application. Finite Element Method Magnetics (FEMM) are used to illustrate the magnetic circuit design analysis of the isolator. Finally, the variation in the magnetic field due to varies the current input is discussed. To conclude, a series of preliminary experimental testing is conducted to evaluate the vibration isolator.

Design of MREs vibration isolator

There are two acknowledged MR mount concepts with high-frequency regions that be adapted to provide a novel MREs isolator. The first concept was proposed by Choi and co-workers [20] that using mixed-mode operation between flow and shear mode. The second concept was introduced by Nguyen et al. [21] that could generate a high damping force featuring MR valve structure. The mixed-mode MR mount concept is observed to exhibit favorable vibration elimination performance in the local resonance frequency. In this concept, the mixed mode operation MR mount comprises two main elements which are rubber and MR dash-pot. MR dash-pot is the part that consists of MR fluid, piston, an electromagnetic coil, flux guide and housing. The electromagnetic coil was wound inside the cylindrical housing. The primary role of rubber element is to support the static load and isolate the vibration transmission at the non-resonant state. There are two parts of the mount which divided into top and bottom sections. The top section that made of rubber element and upper base that fastened to the body and support rubber element while the bottom part mainly consists the mount body.

Learning from these examples, the principles of isolation improvement in the MREs isolator mainly can be done by maximizing the storage modulus or stiffness of MREs in a large effective area. The effective area of MREs is the area where the activation of the magnetic field can effectively regulate the rheological properties of MREs. The stiffness of MREs can be augmented by increasing the magnetic flux density. However, the magnetic flux density is highly related to the current supplied to the coil and permeability of magnetic material as a looping medium. If the utilization of high permeability material is exempted, the typical consequences of increasing

magnetic flux density are higher dimensions of the coil, which lead to a larger size of MREs isolator, and higher power consumption.

Figure 1 illustrates the design concept of MREs isolator by referring to the design mentioned above. The design has been modified by introducing a single mode rather than a mixed mode with the most straightforward configuration by putting coils at the center part to generate magnetic circuits at the top and bottom of the MREs isolator. From the first design concept, a modified version was made by replacing the rubber element with MREs and eliminating MR fluid in the dash-pot element. The MREs replaces the role of the rubber element to support the static load and isolated the vibration at high frequency. In this design, the MREs isolator consists of MREs mount, shaft, an electromagnetic coil, coil bobbin, and housing. The aim of eliminating MRF in this design is to avoid sedimentation. In the meantime, the design structure of the proposed MREs isolator is slightly the same as the second design concept. From these designs, the upper part of the isolator is mirrored to the bottom part of the isolator by minimizing the complexity of the design.

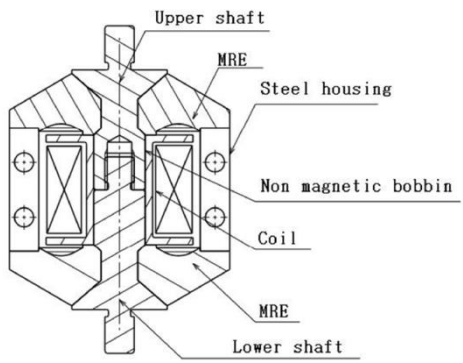

Figure 1. Proposed MREs vibration isolator with cone shape MREs.

The conceptual design of MREs isolator consists of seven parts including an upper shaft, MREs mounts, housing, coil bobbin, coil and lower shaft as labeled in the figure above. The advantage of using the same configuration for top and bottom part of the oscillator is that the stiffness for both sides is evenly, and, consequently, the isolator can be placed in various directions based on requirement. The stiffness variation of the MREs based isolator depends on the region of the effective area. A more significant effective area is needed to increase and maximize the stiffness of isolator. To significantly tune the stiffness, the region of flux guide should have high magnetic intensity. Therefore, such configuration of the isolator was designed, which could be used to dissipate the unwanted vibration.

Magnetic circuit analysis

The capability of the designed electromagnetic device was confirmed initially using magnetic circuit analysis. According to the magnetostatic principle, the flux lines enter and leave a particular region should assure that they flow across the test area in such a way evenly distributed and strong enough. Figure 2 displays the simplification of electromagnetic design into a flexible circuit. Coil expressed by electromotive forces generate the magnetomotive force, F. The magnetic resistance of each section is shown by reluctance (R). The symbols R_1, R_2, R_{MREs1},R_{MREs2}, and R_3, represent the reluctance of upper shaft, reluctance upper part of MREs sample, reluctance housing, the reluctance of lower shaft and reluctance of lower part MREs, respectively.

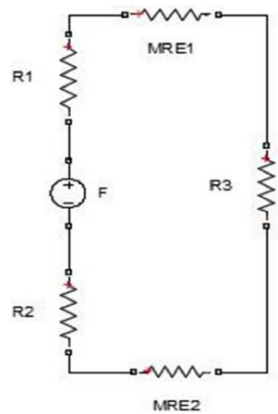

Figure 2. Magnetic circuit diagram

The reluctance of each section can be determined by Eqn. 1 as follows,

$$R = \frac{L}{\mu A} \quad \text{..... (1)}$$

where, L is effective length passed by the magnetic flux in each section, μ is the magnetic permeability, and A is the effective area of the magnetic flux line passing. Based on the circuit, all reluctances of the electromagnetic device are analogous to series of resistant. Therefore, the total can be the summation of all reluctances stated in Eqn. 2

$$\Sigma R = R_1 + R_{MRE1} + R_2 + R_{MRE2} + R_3 \quad \text{..... (2)}$$

Meanwhile, the total electromotive force as expressed in Eqn. 3,

$$\Sigma F = \Phi \Sigma R = NI \quad \text{.....(3)}$$

where, ϕ, N, and I are magnetic flux, some wire turns in each coil, and the current passing through the coils, respectively.

Material selection

The most critical issues in designing the magnetic circuit of the MREs isolator is to form an enclosed magnetic path with high permeability material. Therefore, the consideration of the materials for each component as well as the consideration of coil properties, isolator size, and elastomer types is needed to facilitate the design process.

Table 1. Material selection of isolator component.

No	Isolator part			Remarks
	Housing	Coil bobbin	Shaft	
1	Magnetic	Magnetic	Magnetic	Flux encircles through the housing, coil bobbin and shaft
2	Magnetic	Magnetic	Non- magnetic	Flux encircles through the housing and coil bobbin
3	Magnetic	Non- magnetic	Magnetic	Flux encircles through housing and shaft with high magnetic intensity in MREs
4	Magnetic	Non- magnetic	Non- magnetic	Flux encircle through the housing, coil bobbin, and MREs with high flux leaking in the circuit
5	Non-magnetic	Magnetic	Magnetic	Flux encircles through the coil bobbin and shaft with low flux intensity in MREs
6	Non-magnetic	Magnetic	Non- magnetic	Flux encircles through the coil bobbin
7	Non-magnetic	Non- magnetic	Magnetic	Flux encircles through the shaft and MREs with low magnetic intensity
8	Non-magnetic	Non- magnetic	Non- magnetic	Flux encircle through the housing, coil bobbin, shaft and MREs with uneven magnetic intensity

To select the materials for the component, the clear understanding of flux routing is necessitated. The combination of the materials with high

permeability and low permeability will influence to route the flux path penetrates the MREs mount. To investigate the importance of material for each component, comparative studies on eight possible material arrangement are explored and presented in Table 1. The primary goal of these combinations is to find the better material selection that capable to guide the flux passing through the elastomer mount with sufficient magnetic field strength. From these eight possible combinations, only one combination show the possibility of flux to pass through the elastomer mount with high saturation.

The combination of magnetic housing and shaft with non-magnetic coil bobbin is capable of providing high magnetic field strength in the elastomer mounts. From the remarks in Table 1, it can be resolved that to guide the flux to pass through the elastomer mounts, the permeability of the shaft should be higher than the permeability of the coil bobbin. However, to get a higher magnetic field strength in the elastomer mounts, the permeability of the housing should be at least similar to the permeability of the shaft

In this study, the selection of the housing and shaft is the mild steel that complies with AISI 1020. The design of the housing consists of two identical parts, which each part has two threaded holes as the holder for the locking bolts. Since the coil bobbin has to be made from low permeability material, aluminum is chosen as the material with an O-ring pattern designed. Meanwhile, the shaft is made up of male and female part which also made from mild steel AISI 1020. The detailed material list each of part is shown in Table 2.

Table 2. List of parts and materials for the isolator.

Part No.	Part Name	Type of Material	Material	Type
1	Upper Shaft	Magnetic	Low carbon steel	1020
2	Lower Shaft	Magnetic	Low carbon steel	1020
3	Coil	Non-magnetic	Copper wire	22 SWG
4	Coil Bobbin	Non-magnetic	Aluminium	1100
5	Mounting	MR Material	Elastomer	MREs
6	Housing	Magnetic	Low carbon steel	1020

The outer diameter of the isolator is determined of 60 mm with an overall length of 76 mm. The inner diameter of the coil bobbin that becomes the shaft size is determined of 15 mm. The shaft parts are then formed moveable component alternately in such a way its influence by the elastomer stiffness. As one of the subjects of the research, the current applied varies

from 0 to 1.0 Amps. Since the isolator is designed to generate higher stiffness and load, the shaft and housing should be strong enough to withstand such load, and for that purpose, the thickness of the house is designed about 7.0 mm. As a consequence, the space available for the coil winding that employs 22 SWG copper wire is sufficient for around 491 turns with a total resistance of about 4.96 Ohm. In this research, the current input is limited 1.05 Amps. Therefore, the maximum power consumptions of the isolator are also limited to approximately 2.0 Watts. The dimension of the coils used in this study was chosen based on the higher values of magnetic field intensity, H, which could be achieved by changing the applied current. It seems that that 22 SWG copper wire has the highest value of magnetic field intensity with the average amount of 20771 H.

Magnetic field analysis

The purpose of the electromagnetic circuit design simulation in the MREs isolator was to produce saturated magnetic flux density across the MREs especially at the effective areas. The simulation was conducted using FEMM software. MREs material used in these devices composed of carbonyl iron particles and ground tire rubber with a mass ratio of 27.5 g: 27.5 g. The thickness of the MREs cone is 17 mm, and there are two cones in the device. The magnetic property of the MREs material was obtained from vibrating sample magnetometer (VSM). The B-H curve is depicted in Figure 3. The relationship between magnetic flux density and magnetic field intensity was found to fit a linear relationship that can be defined as R2 >0.99. This relationship also found in Lerner and Cunefare [15] study. The magnetic property in other parts of the device, including housing, shafts, coil bobbin and coil wire can be found with the software.

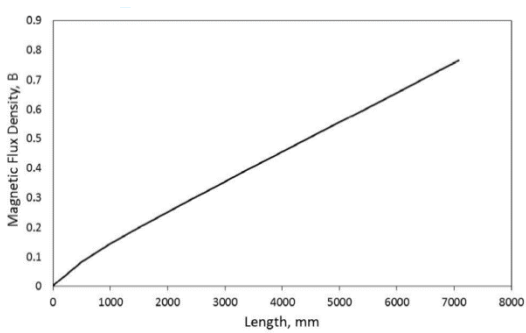

Figure 3. B-H curve used in the FEMM simulation.

Figure 4 shows two-dimensional axisymmetric meshed models in FEMM using triangular elements with a total number of 19628 and a total

node number of 10015. Figure 5 shows the simulated magnetic intensity distribution for the whole magnetic circuit. Notes should be taken that the flux can influence modulus of MREs is only the flux that passed through MREs mountings. The MREs mountings that crossed by the magnetic flux is known as the effective area. According to Figure 5, it can be observed that the flux lines have passed across the upper shaft, lower shaft, and housing. Therefore, the rheological influenced by changing of the current input only occurred in MREs when the flux passed through these three elements. Meanwhile, the coil bobbin is not intensively exposed to a magnetic field, and therefore the influence of magnetic field to the modulus of MREs areas can be neglected. Nevertheless, more focus should be taken at the flux lines in the upper shaft and lower shaft since the structural configuration of these elements formed a parallel channel for the flux lines. Thus, if flux loss is neglected, the total number of magnetic flux that passed through the upper shaft and lower shaft is equal to the amount of magnetic flux that passed through the housing and MREs. It is why the center part of the shaft has higher magnetic flux density than the housing and MREs.

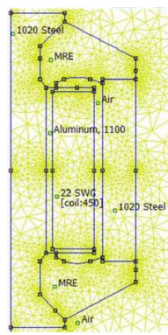

Figure 4. Two dimensional axisymmetric model in FEMM.

According to Table 1, the magnetic flux density is measured across the MREs concerning material selection in number 3. The average values of magnetic flux density were taken in vertical, horizontal and inclined at the effective area of mounting which was indicated by a red dashed line as shown in Figure 6. The software package was related to the type of material of each component of the MREs isolator, type of coil, the number of coil turns winding around the shaft and the amount of the electric current supplied in the coils. These parameters were essential to producing the best value of magnetic field intensity H, which was correlated with the magnetic flux density, B.

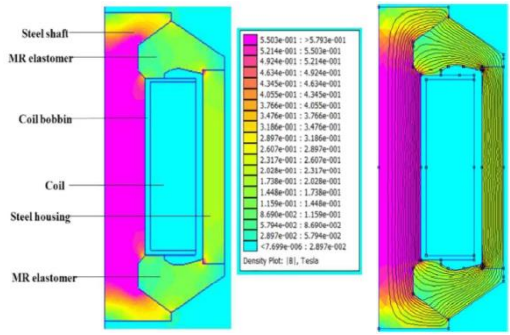

Figure **5**. Magnetic flux distribution.

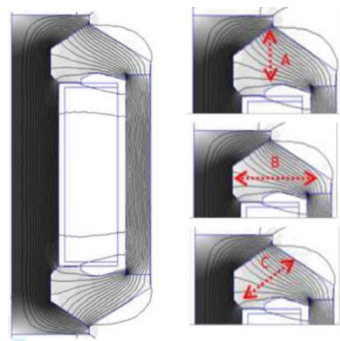

Figure 1. Red line indication of magnetic flux measurement in effective areas.

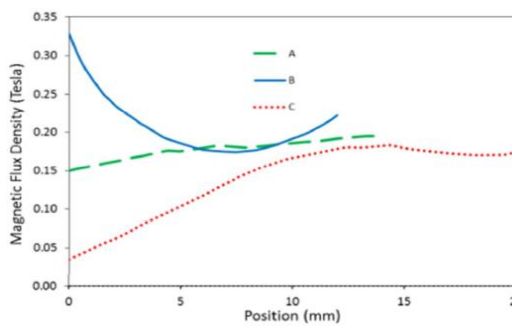

Figure 7. Magnetic flux density measurement.

From Figure 7, the average magnetic flux density at area A, B, and C was 199, 133, and 171 mT, respectively. It was apparent that the highest magnetic flux density occurred at line A, which was parallel to the movement of the shaft. Hence, line A, which was represented the value of magnetic field

density in the vertical direction, was the primary concern as its rheological properties could be effectively regulated by a magnetic field [4]. To prove that the magnetic flux increases as increasing the applied current, the magnetic field strength was measured again in line A, B, and C by varying the amount of used current for design number 3.

Magnetic field analysis is conducted by varying the input current to the isolator. Figure 8 illustrates the values of the magnetic flux density for different amounts of applied currents penetrate through MREs at three different effective areas. From Figure 8, it observes that the magnetic flux density generated at all-area increase with the increasing of applied current from 0.25 to 1.0 Amps. It was clearly remarked that the magnetic field increases as the applied current increase.

In Figure 8 (a), the curves of flux density tended to decrease slowly till reach the lowest point of magnetic field strength and then increase till the end of measurement points. While in Figure 8 (b), the curves are slowly growing till reach the highest position of magnetic field strength and then decrease till the end of measurement points. The result in Figure 8 (c) shows that the curves are slowly decreased from the highest position of magnetic field strength to the lowest point of the magnetic field and then gradually increase until the end of measurement points. It happens due to the magnetic concentration and permeability is higher in the measurement area which nearest to the magnetic material.

Therefore, in other words, the proposed MREs base isolator was designed to maximize the ample magnetic flux density through MREs to gain the maximum stiffness that varies under applied current. Since MREs stiffness is dependent on the magnetic field, the applied current plays a primary role to change the stiffness. As the magnetic field strength increases, the stiffness of MRES can be significantly increasing [5].

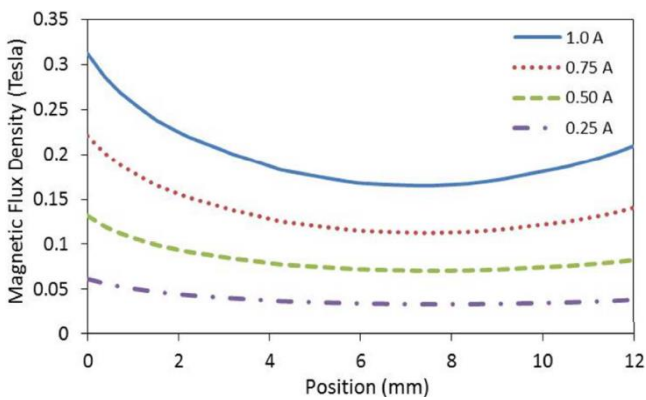

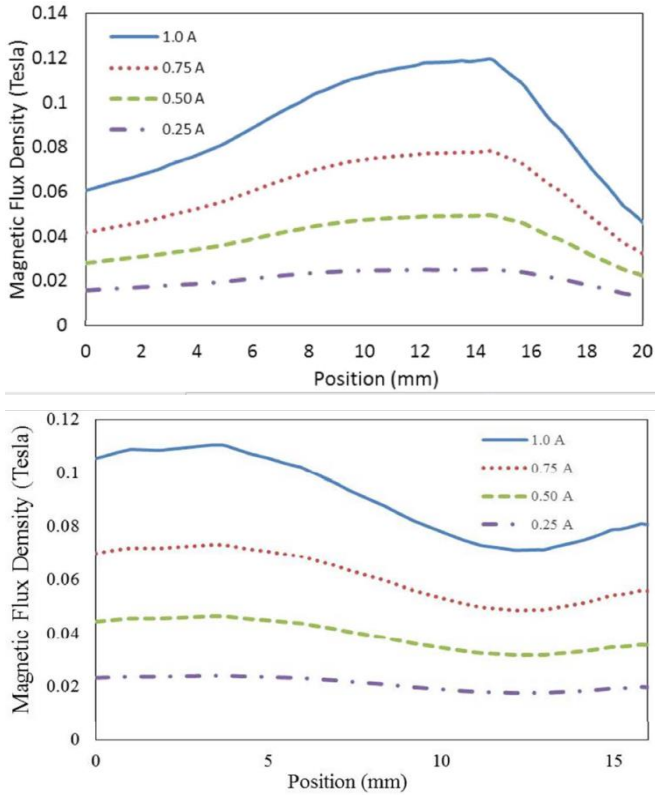

Figure 8. Simulated magnetic flux density versus length for different applied current at (a) area A, (b) area B and (c) area C.

MREs Fabrication

The fabrication of the MREs samples involved two major steps; mixing and curing. Since the MREs used in this study is the isotropic type, the sample is prepared under a natural condition in the absence of magnetic field. Two samples of dia. 60 x 17 mm with same ingredients were fabricated. The ingredients used in the fabrication consists of carbonyl iron particles (CIP) and ground tire rubber (GTR) with a mass fraction of 50% and 50% respectively. A mixer was utilized for mixing CIP and GTR powder at 250 rpm. In the first step of the fabricating process, the CIP (C3518; Sigma-Aldrich Pty. LTD; ≥ 97% Fe basis) with 3-5μm size distribution are mixed into the GTR in a mixer about 10-15 minutes at 250 rpm.

The molding was then mounted in the high-temperature high pressure (HPHT) device as shown in Figure 9 and resulted in MREs samples as shown in Figure 10. The mixture of MREs sample was performed by applying a

hydraulic pressure of 15 bar to the molding followed by heating in 200°C. This heating step was kept off an hour. The hot mold was then allowed to cool until reaching ambient temperature.

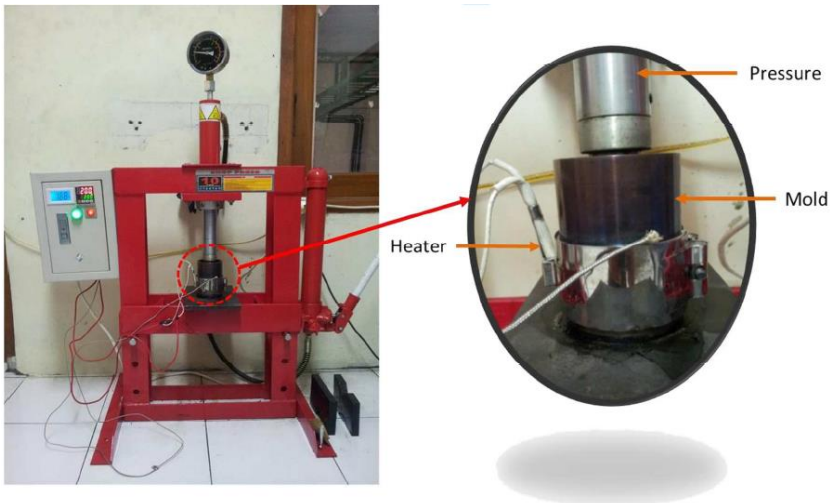

Figure 9. HPHT fabrication device.

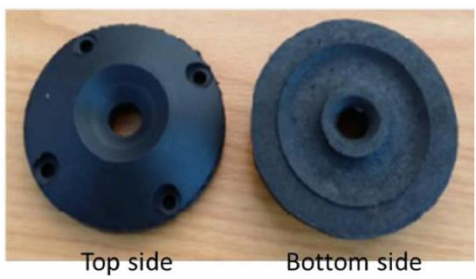

Figure 10. MREs samples.

Preliminary Experiment

The experimental setup consisted of six main components as presented in Figure 11. The isolator was attached to the testing machine (Shimadzu Hydraulically actuated Fatigue Dynamic Test Machine) that equipped with a 20 kN force sensor and a displacement sensor. The device was connected to a data logger to record the results. In the experiment, the MREs isolator was connected to a power supply to generate a varying magnetic field. The testing

machine was operated in a vertical direction to obtain forces and displacement response under compression mode. The test was performed with off-state and on-state at 2.0 Amps current at 0.5 mm amplitude.

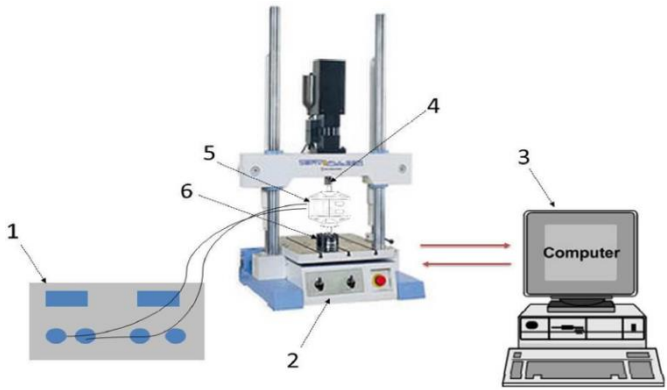

Figure 11. Schematic diagram for the experimental setup. 1. Controllable power supply, 2. Shimadzu Fatigue Dynamic Test Machine, 3. Computer, 4. Exciter, 5. Prototype, 6. Load Cell.

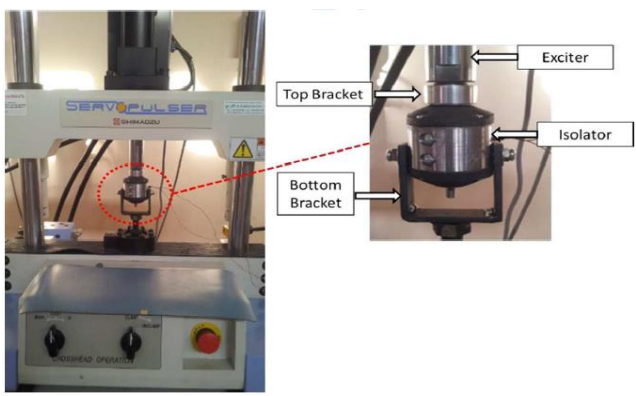

Figure 12. Experimental setup for testing the MREs isolator.

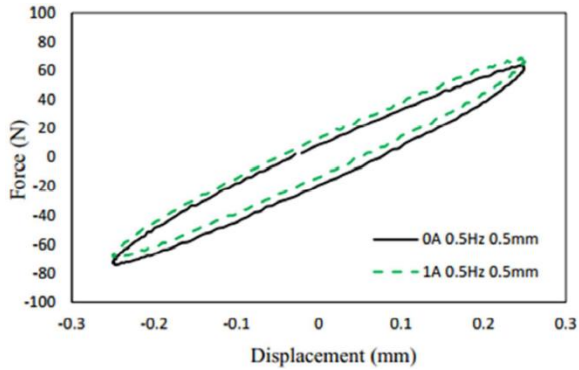

Figure 13. Force-displacement loops of MREs isolator at amplitude 0.5 mm and frequency 0.5 Hz.

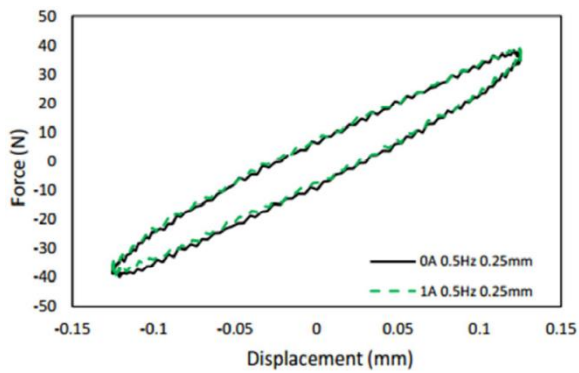

Figure 14. Force-displacement loops of MREs isolator at amplitude 0.25 mm and frequency 0.5 Hz.

Figure 13 shows the force-displacement loops of the MREs isolator when the amplitude of the sinusoidal motion of the exciter is 0.50 mm, and the frequency is 0.5 Hz. Figure 14 shows the force-displacement loops of the MREs isolator when the amplitude of the sinusoidal motion of the exciter is 0.25 mm, and the frequency is 0.5 Hz. There is an apparent increment in the force when the applied current rise from 0 to 1A under off-state and on-state condition respectively. The maximum force increase happens when the amplitude of the sinusoidal motion of exciter in 0.5 mm and the frequency is 0.5 Hz. From both figures, it can be noted that the force-displacement loops follow clockwise paths and it is clearly observed the effects of changing magnetic field. The loops of force-displacement of MREs isolator also shows that it behaves as a stiffness varying element.

The maximum force generated from the MREs isolator increase from 64.2 N (off-state, I=0A) to 69.4 N (on-state, I=1A), equivalent to 8% increase. While at amplitude 0.25 mm, the force is increased about 1-2% from off-state to on-state. The peak force value force both amplitude motion is listed in Table 3. As can be seen, there is a significant increase in the force generated by the MREs isolator at the on-state as compared to the off-state condition. It shows that the maximum force of the isolator exhibit a linear relationship with the current input.

Table 3. Force [N] of the MREs isolator under 0.5 Hz frequency at different amplitude condition.

Amplitude	OFF-state (I=0A)	ON-state (I=1A)
0.5	64.2	69.4
0.25	38.6	39.1

Figures 15 and 16 deliver the comparison of the force-displacement loops for a fixed applied current with varying amplitude of excitation. A correlation between the force-displacement loops of MREs isolator at different amplitude 0.5 and 0.25 mm for a given frequency of 0.5 Hz at 0 A is presented in Figure 15. While the comparison between the force-displacement loops of MREs isolator at different amplitude 0.5 and 0.25 mm for a given frequency of 0.5 Hz at 1 A current is presented in Figure 16. As the isolator is acting as an elastic spring, the force output tends to increase as the loading amplitude is increasing. Conversely, the gradient of the loops for both force-displacement loops is remain equivalent when magnifying the amplitude of the excitation input from 0.25 to 0.5 mm. Even though that all the tests were conducted in a small displacement range, it still can be concluded that the isolator can works in its elastic range greater than 0.5 mm. In conclusion, it can be realized that the stiffness of MREs isolator is changing as the application of magnetic field by referring the force-displacement loop.

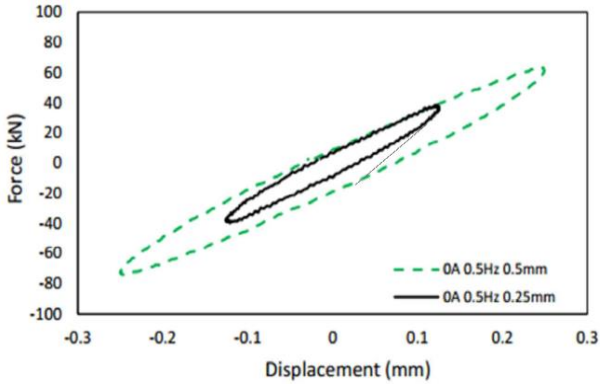

Figure 15. Force-displacement loops of the MREs isolator at frequency 0.5Hz and amplitudes of 0.25 and 0.5 mm at 0 A.

Capable of rapidly changing its stiffness by activating the magnetic field, this MREs isolator is capable of making known as substantial adaptability into the isolator in order to overcome the limitations associated with conventional isolators.

Conclusion

A step by step development of cone-shaped MREs based isolator has been delivered in a logical order of design. A magnetic circuit was developed to predict the magnetic flux inside. The prediction was then confirmed using FEMM simulation. The cone shape MREs and steel shaft serve as the magnetic cores together with the steel housing. The impact of each part of the magnetic circuit was investigated carefully. In particular, variation in the magnetic field due to the applied current is discovered. It is found that the changes of current may cause a change in the magnetic field of the isolator. The steps should be considered during the designing stage of MREs isolator. The prototype was fabricated and tested to prove the stiffness changing. Based on the experimental test, the stiffness changing can be determined from the force-displacement curves. Although, it was a slight change, the first prototype has proved the concept and it should be deeply reinvestgated in the near future.

Acknowledgment

The authors are grateful to the Universitas Sebelas Maret for Hibah Kolaborasi Internasional 2017 and Universiti Teknologi Malaysia. This

research is also partially funded by SHERA program through Prime Award: AID-497-A-16-00004, USAID

References

[1] Li, W., Zhang, X. and Du, H. "Development and Simulation Evaluation of a Magnetorheological Elastomer Isolator for Seat Vibration Control", Journal of Intelligent Material Systems and Structures, 23(9), pp. 1041–1048 (2012).

[2] Li, W. H. Zhou, Y. and Tian, T. F. "Viscoelastic Properties of MR Elastomers under Harmonic Loading", Rheologica Acta, 49(7), 733–740 (2010).

[3] Zhou, G. Y. and Jiang, Z. Y. "Deformation in Magnetorheological Elastomer and Elastomer–ferromagnet Composite Driven by a Magnetic Field", Smart Materials and Structures, 13(2), pp. 309–316 (2014).Hutchinson, F. David and M. Ahmed, *U.S. Patent No. 6,912,127* (28 June 2005).

[4] Zhou, G. Y. "Shear Properties of a Magnetorheological Elastomer", Smart Materials and Structures, 12: 139–146, pp. (2003).

[5] Fuchs, A., Zhang, Q., Elkins, J., Gordaninejad, F. and Evrensel, C. "Development and Characterization of Magnetorheological Elastomers", Journal of Applied Polymer Science, 105(5), pp. 7–11 (2007).

[6] Ginder, J. M., Clark, S. M., Schlotter, W. F., Nichols, M. E., and Company, F. M. "Magnetostrictive Phenomena in MRE", International Journal of Modern Physics B, 16, pp. 2412–2418 (2002).

[7] Wang, X. and Cai, J. "Magnetorheological Elastomer : State and Application", Advanced Material Research, 395, pp. 161–165 (2012).

[8] Kaleta, J., Królewicz, M., and Lewandowski, D. "Magnetomechanical Properties of Anisotropic and Isotropic Magnetorheological Composites with Thermoplastic Elastomer Matrices", Smart Materials and Structures, 20(8), pp. 085006 (2011).

[9] Gordaninejad, F., Wang, X., and Mysore, P. "Behavior of Thick Magnetorheological Elastomers", Journal of Intelligent Material Systems and Structures, 23(9), pp. 1033– 1039 (2012).

[10] Li, Y., Li, J., Li, W., and Samali, B. "Development and Characterization of a Magnetorheological Elastomer Based Adaptive Seismic Isolator", Smart Materials and Structures, 22(3), pp. 035005 (2013).

[11] Fu, J., Zheng, X., Yu, M., Ju, B. X., and Yang, C. Y. "A New Magnetorheological Elastomer Isolator in Shear - Compression Mixed Mode", Journal of Intelligent Material Systems and Structures, pp. 1702–1706 (2014).

[12] Li, Y., Li, J., Li, W., and Du, H. "A State-of-the-Art Review on Magnetorheological Elastomer Devices", Smart Materials and

Structures,. 23, pp. 123001 (2014).
[13] Ubaidillah, Sutrisno, J., Purwanto, A. and Mazlan, S. A. "Recent Progress on MR Solids : Materials, Fabrication, Testing and Applications", Advanced Engineering Materials,. 17(5), pp. 563–597 (2015).
[14] Lerner, A. A. and Cunefare, K. A. "Performance of MRE-Based Vibration Absorbers", Journal of Intelligent Material Systems and Structures, 19(5), pp. 551–563 (2007).
[15] Behrooz, M., Wang, X., and Gordaninejad, F. "Modeling of a New Semi-Active Passive Magnetorheological Elastomer Isolator", Smart Materials and Structures, 23, pp. 045013 (2014).
[16] Deng, H. and Gong, X. "Application of Magnetorheological Elastomer to Vibration Absorber", Communications in Nonlinear Science and Numerical Simulation, 13(9), pp. 1938–1947 (2008).
[17] Liao, G. J., Gong, X. L., Kang, C. J., and Xuan, S. H. "The Design of an Active–adaptive Tuned Vibration Absorber Based on Magnetorheological Elastomer and Its Vibration Attenuation Performance", Smart Materials and Structures, 20(7), pp. 075015 (2011).
[18] Opie, S. and Yim, W. "Design and Control of a Real-Time Variable Stiffness Vibration Isolator", IEEE/ASME International Conference on Advanced Intelligent Mechatronics, pp. 380–385 (2009).
[19] Van Engelen, N. C., Osgooei, P. M., Tait, M. J., and Konstantinidis, D. "Experimental and Finite Element Study on the Compression Properties of Modified Rectangular Fiber-Reinforced Elastomeric Isolators (MR-FREIs)", Engineering Structures, 74, pp. 52–64 (2014).
[20] Choi, S. B., Hong, S. R., Sung, K. G., and Sohn, J. W. "Optimal Control of Structural Vibrations Using a Mixed-Mode Magnetorheological Fluid Mount", International Journal of Mechanical Sciences, 50(3), pp. 559–568 (2008).
[21] Nguyen, Q. H., Choi, S. B., Lee, Y. S., and Han, M. S. "Optimal Design of High Damping Force Engine Mount Featuring MR Valve Structure with Both Annular and Radial Flow Paths", Smart Materials and Structures, 22, pp. 115024 (2013).